J Arid Land (2023) 15(11): 1315–1339
https://doi.org/10.1007/s40333-023-0069-5

Science Press Springer-Verlag

Spatiotemporal variation of surface albedo and its influencing factors in northern Xinjiang, China

YUAN Shuai[1,2], LIU Yongqiang[1,2*], QIN Yan[1,2], ZHANG Kun[1,2]

[1] College of Geography and Remote Sensing Sciences, Xinjiang University, Urumqi 830046, China;
[2] Xinjiang Key Laboratory of Oasis Ecology, Xinjiang University, Urumqi 830046, China

Abstract: Surface albedo is a quantitative indicator for land surface processes and climate modeling, and plays an important role in surface radiation balance and climate change. In this study, by means of the MCD43A3 surface albedo product developed on the basis of Moderate Resolution Imaging Spectroradiometer (MODIS), we analyzed the spatiotemporal variation, persistence status, land cover type differences, and annual and seasonal differences of surface albedo, as well as the relationship between surface albedo and various influencing factors (including Normalized Difference Snow Index (NDSI), precipitation, Normalized Difference Vegetation Index (NDVI), land surface temperature, soil moisture, air temperature, and digital elevation model (DEM)) in the north of Xinjiang Uygur Autonomous Region (northern Xinjiang) of Northwest China from 2010 to 2020 based on the unary linear regression, Hurst index, and Pearson's correlation coefficient analyses. Combined with the random forest (RF) model and geographical detector (Geodetector), the importance of the above-mentioned influencing factors as well as their interactions on surface albedo were quantitatively evaluated. The results showed that the seasonal average surface albedo in northern Xinjiang was the highest in winter and the lowest in summer. The annual average surface albedo from 2010 to 2020 was high in the west and north and low in the east and south, showing a weak decreasing trend and a small and stable overall variation. Land cover types had a significant impact on the variation of surface albedo. The annual average surface albedo in most regions of northern Xinjiang was positively correlated with NDSI and precipitation, and negatively correlated with NDVI, land surface temperature, soil moisture, and air temperature. In addition, the correlations between surface albedo and various influencing factors showed significant differences for different land cover types and in different seasons. To be specific, NDSI had the largest influence on surface albedo, followed by precipitation, land surface temperature, and soil moisture; whereas NDVI, air temperature, and DEM showed relatively weak influences. However, the interactions of any two influencing factors on surface albedo were enhanced, especially the interaction of air temperature and DEM. NDVI showed a nonlinear enhancement of influence on surface albedo when interacted with land surface temperature or precipitation, with an explanatory power greater than 92.00%. This study has a guiding significance in correctly understanding the land-atmosphere interactions in northern Xinjiang and improving the regional land-surface process simulation and climate prediction.

Keywords: surface albedo; MCD43A3; Hurst index; random forest (RF) model; geographical detector (Geodetector); Normalized Difference Snow Index (NDSI); northern Xinjiang

Citation: YUAN Shuai, LIU Yongqiang, QIN Yan, ZHANG Kun. 2023. Spatiotemporal variation of surface albedo and its influencing factors in northern Xinjiang, China. Journal of Arid Land, 15(11): 1315–1339. https://doi.org/10.1007/s40333-023-0069-5

*Corresponding author: LIU Yongqiang (E-mail: liuyq@xju.edu.cn)
Received 2023-02-21; revised 2023-08-09; accepted 2023-08-13

1 Introduction

Surface albedo refers to the ratio of reflected radiation to the total incident radiation on the Earth's surface (Dickinson, 1983). It is a key regulating variable of radiation budget on the Earth's surface (Bonan, 2008) and an important quantitative indicator in the study of land-surface process simulation and climate prediction (Liang et al., 2019). Surface albedo plays an important role in the land-atmosphere system. The conditions of the underlying surface (vegetation cover, soil moisture, etc.) and meteorological factors (precipitation, air temperature, etc.) directly or indirectly affect surface albedo (Wielicki et al., 2005; Gorelick et al., 2017), thereby affecting the transfer of surface fluxes (sensible heat, latent heat, and soil heat flux) and regional atmospheric circulation, resulting in significant climatic effects locally and even globally (Rotenberg and Yakir, 2010). Therefore, a comprehensive understanding of the variation characteristics of surface albedo is essential for studying the land surface processes, climate change, etc. (Cess, 1978; Ollinger et al., 2008; Van De Kerchove et al., 2013, Hotaling et al., 2021).

Under the assistance of remote sensing satellites, some surface albedo products with global coverage based on the Moderate Resolution Imaging Spectroradiometer (MODIS) (Lucht et al., 2000; Schaaf et al., 2002), Global Land Surface Satellite (GLASS) (Liang et al., 2013; Liu et al., 2013), GlobAlbedo (Potts et al., 2012), etc., have been produced. They can provide long-term time series data to study the spatiotemporal distribution characteristics of surface albedo and its evolution pattern on a large scale. Among them, the MODIS-based surface albedo products have been widely and effectively used due to their excellent quality and spatiotemporal continuity (Wang et al., 2012; Wang et al., 2014b; Wen et al., 2022). In terms of influencing factors of surface albedo, previous studies have shown that surface albedo change is correlated with ecological or meteorological parameters (He et al., 2014), such as snowpack (Loranty et al., 2014), land surface temperature (Shekhar et al., 2010), and soil moisture (Verheijen et al., 2013), and has strong seasonal variation (Fang et al., 2007; Shi and Liang, 2013) featured by a decreasing trend in July and an increasing trend in January (He et al., 2014).

Studies related to surface albedo in China have mainly focused on the Qinghai-Tibet Plateau and central and eastern China (Wang et al., 2005; Tang et al., 2018; Huang et al., 2019; Chen et al., 2021), while fewer studies have been conducted in Xinjiang Uygur Autonomous Region in Northwest China. Xinjiang has diverse climate types and ecological environments, as well as complex topography and landscapes in spatial and temporal distribution (Li et al., 2018). It can be divided into two major parts, i.e., northern Xinjiang and southern Xinjiang, by the major ridgelines of the Tianshan Mountains. Northern Xinjiang is a typical arid and semi-arid region, dominated by a continental climate, with little precipitation, strong evaporation, and sparse vegetation (Wang et al., 2014a; Zhang et al., 2021a). The sensitive underlying surface characteristics in this region can timely reflect the regional climate change of dry, wet, and cold-warm processes (Alessandri et al., 2021). The land cover types in northern Xinjiang are more complex, including cropland, forestland, grassland/shrubland, wetland, water bodies, impervious surface, bare land, and snow/ice. This complexity allows for the study of the variation characteristics of surface albedo under diverse land cover types, in which the change in snowpack contributes more to the variation in surface albedo than other factors (Pang et al., 2022). Northern Xinjiang is one of the three major snowpack distribution areas in China (Wang et al., 2008; Zhang et al., 2021a), making it an ideal location for studying the effect of snowpack on surface albedo. Approximately 20%–70% of surface water in northern Xinjiang comes from snowmelt and glacier meltwater (Kong and Pang, 2012). According to the estimation of glacier surface summer albedos and snowmelt model, the reduced surface albedo can drive about 30%–60% of glacier melting on the Tibetan Plateau and its surrounding regions (Zhang et al., 2021b). Therefore, it is crucial to study the variation characteristics of surface albedo and analyze its influencing factors in northern Xinjiang to reveal the patterns of snowmelt and glacier meltwater, predict snowmelt floods, and assess water supply and demand. Compared to southern Xinjiang, human activities are more concentrated in northern Xinjiang and have a relatively significant impact on impervious surface of construction land. Future change in surface

albedo caused by urbanization is one of the causes of global warming (Ouyang et al., 2022). Studying these natural and human effects can provide a deeper understanding on the causes of surface albedo change. However, previous studies on surface albedo in northern Xinjiang were only conducted on a small spatial scale (Deng et al., 2021), and the spatiotemporal distribution and influencing factors have not been well documented.

For these reasons, this study characterized the spatiotemporal variation of surface albedo in northern Xinjiang using the daily MODIS-based MCD43A3 surface albedo product, and quantitatively analyzed the influencing factors of surface albedo, including Normalized Difference Snow Index (NDSI), precipitation, Normalized Difference Vegetation Index (NDVI), land surface temperature, soil moisture, air temperature, and digital elevation model (DEM). The specifics include the following three processes. First, the spatial distribution and variation trend of surface albedo, as well as the correlation between surface albedo and its influencing factors were investigated using the dimensionality reduction analysis method. Second, by means of the unary linear regression and Hurst index methods, the spatiotemporal variation of surface albedo was independently analyzed, and then the past trend and future change of surface albedo were revealed. Third, based on the correlation analysis between surface albedo and its influencing factors, we used the random forest (RF) model and geographic detector (Geodetector) to jointly quantify the influencing factors of surface albedo, so as to further explore the interrelationships between influencing factors and the influencing mechanisms of surface albedo change in northern Xinjiang. This study has a guiding significance in correctly understanding the land-atmosphere interactions in northern Xinjiang and improving the regional land-surface process simulation and climate change prediction.

2 Materials and methods

2.1 Study area

Northern Xinjiang (79°53′10″–96°22′54″E, 42°15′29″–49°10′59″N) is located in the hinterland of central Asia, north of the main ridge line of the Tianshan Mountains in Xinjiang Uygur Autonomous Region, Northwest China, with an area of about 4.50×10^5 km^2 and an altitude of 185–5457 m (Fig. 1). The region has a typical temperate continental arid and semi-arid climate (Zhang et al., 2019), with large differences in temperature between winter and summer and scarce precipitation throughout the year (Luo et al., 2017). The study area is surrounded by the Tianshan Mountains and Altay Mountains, with the Junggar Basin in the middle part. In the northern basin, there is the Ulungur Lake, the largest inland lake in northern Xinjiang (Zou et al., 2021), and in the western part, there is the Ebinur Lake, the largest brackish water lake in Xinjiang (Wang et al., 2019). The center of the Junggar Basin is the Gurbantunggut Desert, with wide distribution of desert grasslands and deserts, extreme drought, little precipitation, and obvious soil salinization (Wang et al., 2014a; Zhang et al., 2021a).

2.2 Data sources

The data based on the daily-scale MCD43A3 WSA-shortwave surface albedo product with a spatial resolution of 500 m, the daily-scale MOD10A1 NDSI product with a spatial resolution of 500 m, and the MOD13A3 NDVI product with a spatial resolution of 1 km were obtained from Level-1 and Atmosphere Archive & Distribution System Distributed Active Archive Center (LAADS DAAC) (https://ladsweb.modaps.eosdis.nasa.gov). The time range was from December 2009 to December 2020. NDSI can provide snow cover information within MODIS pixels, with an average absolute error of less than 0.1 (Salomonson and Appel, 2004). Due to the high surface albedo (above 0.7) of snow-covered land (which is much higher than that of other land cover types) and the fact that changes in surface albedo of snow-covered land were mainly caused by snow loss rather than snow metamorphism (Qu and Hall, 2007), changing snow cover can greatly affect surface albedo. Therefore, using NDSI as a snow cover indicator is useful for studying the impact of snow on surface albedo.

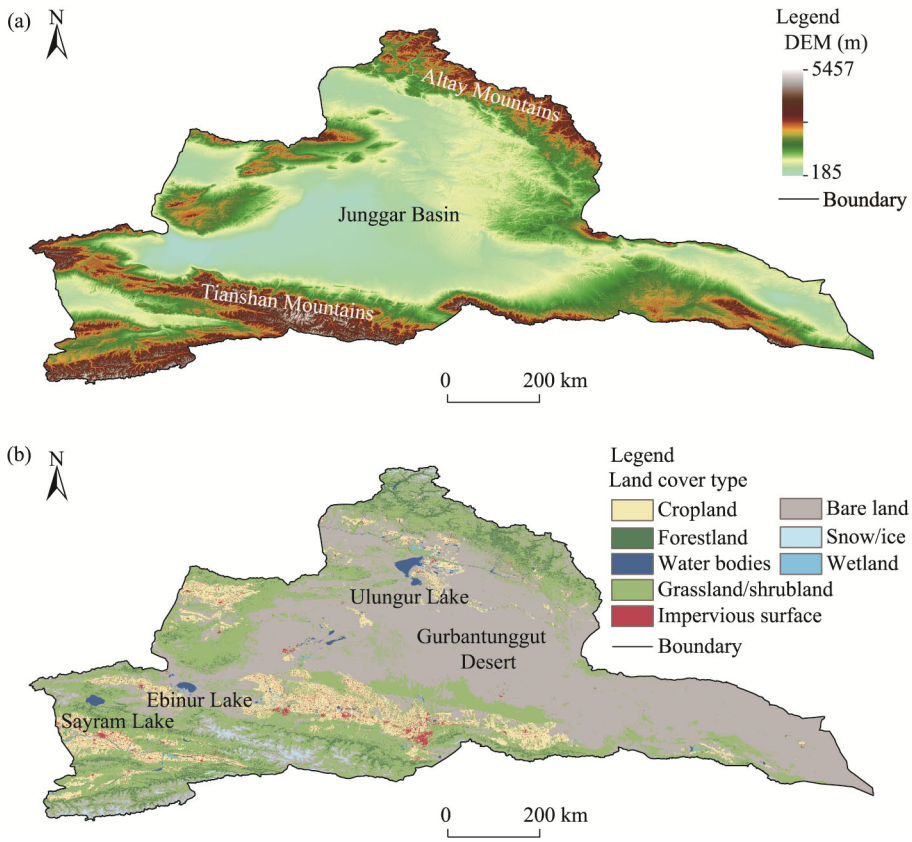

Fig. 1 Overview of northern Xinjiang based on digital elevation model (DEM) (a) and spatial distribution of land cover types in northern Xinjiang in 2020 (b). Note that the figures are based on the standard map (GS (2019) 1822) from the Standard Map Service System (http://bzdt.ch.mnr.gov.cn/index.html), and the standard map has not been modified.

The meteorological datasets including monthly precipitation (mm) and monthly average temperature (°C) from December 2009 to December 2020 were provided by the National Earth System Science Data Center (http://www.geodata.cn), with a spatial resolution of 1 km. The digital elevation model (DEM) data with a spatial resolution of 90 m were provided by the Resource and Environment Science and Data Center (https://www.resdc.cn).

We obtained the land cover data (2020) from the land cover mapping product of Cross-Resolution Land-Cover (CRLC) mapping framework (https://github.com/LiuGalaxy/CRLC) based on noisy label learning, which has a spatial resolution of 10 m. This map was created using a deep classification network, including categories such as cropland, forestland, wetland, grassland/shrubland, water bodies, impervious surface, bare land, and snow/ice. The final assessment on this map showed an overall accuracy of 84.35% (±0.92%) (Liu et al., 2023).

The data on land surface temperature (°C) and soil moisture were obtained from the National Tibetan Plateau Data Center (http://data.tpdc.ac.cn). The data included a daily all-weather land surface temperature dataset with a spatial resolution of 1 km (from December 2009 to December 2020) and a soil moisture dataset with a spatial resolution of 0.05° (from December 2009 to December 2018, missing the data of 2019 and 2020 compared to other datasets).

All data were resampled to a spatial resolution of 500 m, and the monthly, seasonal (spring from March to May, summer from June to August, autumn from September to November, and winter from December to February of the next year), and annual average values of the data in the study area were calculated.

2.3 Methods

2.3.1 Spatial analysis

In order to visually and accurately characterize the spatial distribution of surface albedo, this study conducted a dimensionality reduction analysis to reveal the distribution characteristics of surface albedo on longitude or latitude based on the seasonal and annual average values of surface albedo (Fig. 2a). The formula is as follows:

$$g(x) = \frac{\sum_{y} f(x,y)}{N_y}, \tag{1}$$

where $g(x)$ is the mean function of surface albedo that varies with longitude (or latitude); y is the latitude (or longitude); $f(x, y)$ is the spatial distribution function of surface albedo with latitude and longitude; and N_y is the number of image elements in the direction of latitude (or longitude).

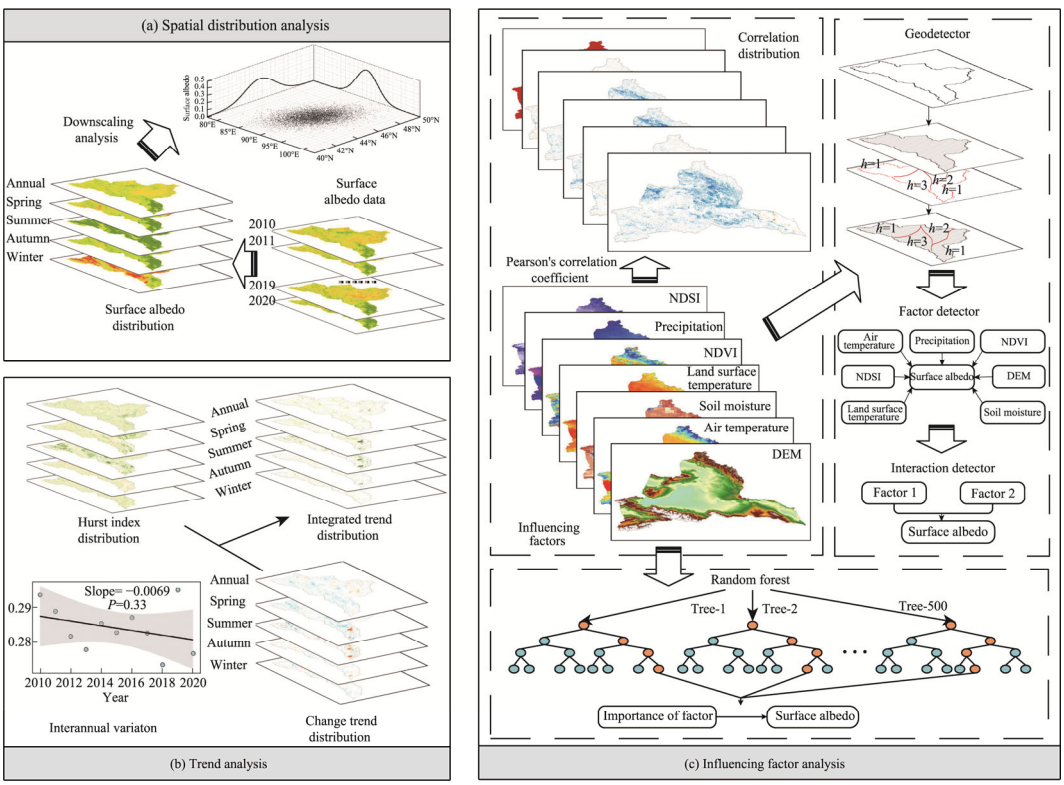

Fig. 2 Flow chart of analysis in this study. (a), spatial distribution analysis; (b), trend analysis; (c), influencing factor analysis. NDSI, Normalized Difference Snow Index; NDVI, Normalized Difference Vegetation Index; Geodetector, geographical detector; *h*, the stratification of surface albedo (or its influencing factors) in the Geodetector.

2.3.2 Trend analysis

The spatial variation trends of surface albedo and its influencing factors (including NDSI, precipitation, NDVI, land surface temperature, soil moisture, and air temperature) were analyzed using the unary linear regression (Tang et al., 2020) and Hurst index (Fan et al., 2012; Hou et al., 2012) methods (Fig. 2). Firstly, the pre-processed (annual and seasonal) average values of surface albedo and its influencing factors were employed to calculate the element-by-element trend, i.e., the slope of the linear trend, by using the unary linear regression method. The significance and reliability of the pixel-by-pixel trend were determined by the *t*-test. Secondly, confidence intervals of 99% (P<0.01) and 95% (P<0.05) were used as thresholds to classify regions with significant changes, and their distributions were analyzed by dimensionality reduction in the direction of

longitude (or latitude). The classification criteria and spatial distribution function values are shown in Table 1, where P>0.05 indicates no significant trend (Knorr et al., 2001). The formula can be expressed as:

$$\text{Slope} = \frac{\sum_{i=1}^{n} X_i i - \frac{1}{n}\left(\sum_{i=1}^{n} X_i\right)\left(\sum_{i=1}^{n} i\right)}{\sum_{i=1}^{n} i^2 - \frac{1}{n}\left(\sum_{i=1}^{n} i\right)^2} \times 10 , \tag{2}$$

where slope is the trend of surface albedo (or its influencing factors) per decade; n is the total number of years; and X_i is the surface albedo (or its influence factors) in the i^{th} year (i=1, 2, ..., n). Slope>0 indicates an increasing trend of surface albedo (or its influence factors); otherwise, surface albedo (or its influence factors) shows a decreasing trend. The larger the absolute value, the faster the increase or decrease rate.

Table 1 Classification criteria and spatial distribution function values for the variation trends of surface albedo and its influencing factors

Spatial variation trend	Slope	P	Spatial distribution function value
Extremely increasing	>0	<0.01	1.00
Intermediately increasing	>0	0.01–0.05	0.50
Extremely decreasing	<0	P<0.01	–1.00
Intermediately decreasing	<0	0.01–0.05	–0.50

The Hurst index was used to quantify the long-term dependence of time-series information based on the Rescaled Range (R/S) analysis (Fan et al., 2012; Hou et al., 2012). The R/S analysis method can effectively calculate the Hurst index according to the following principle.

For a time series $\xi(t)$ (where t is the time; t=1, 2, ..., n), we defined another series τ (τ=1, 2, ..., n); for a certain τ, the average series $\langle\xi\rangle_\tau$ can be defined as (Sánchez-Granero et al., 2008):

$$\langle\xi\rangle_\tau = \frac{1}{\tau}\sum_{t=1}^{\tau}\xi(t) . \tag{3}$$

For time t, the cumulative discrepancy $X(t, \tau)$ can be calculated as:

$$X(t,\tau) = \sum_{i=1}^{t}\left(\xi(i) - \langle\xi\rangle_\tau\right) , \ 1 \le t \le \tau . \tag{4}$$

The range series $R(\tau)$ and the standard deviation series $S(\tau)$ can be defined as Equations 5 and 6, respectively:

$$R(\tau) = \max_{1\le t\le\tau} X(t,\tau) - \min_{1\le t\le\tau} X(t,\tau) , \tag{5}$$

$$S(\tau) = \sqrt{\frac{1}{\tau}\sum_{t=1}^{\tau}\left(\xi(t) - \langle\xi\rangle_\tau\right)^2} . \tag{6}$$

Then, the exponential law can be derived as:

$$\frac{R(\tau)}{S(\tau)} = (c\tau)^H , \tag{7}$$

where H is the Hurst index and c is a constant.

If the exponential law of the Hurst index is satisfied, there is a Hurst phenomenon in the time series $\xi(t)$. As shown in Table 2, there are three main forms of the Hurst index. The closer the Hurst index value to 1.00, the stronger the persistence, and the closer the Hurst index value to 0.00, the stronger the anti-persistence (Hou and Hou, 2020). In this study, the Hurst index was divided into seven levels to analyze the persistence status and the distribution of surface albedo,

and the dimensionality reduction analysis was also used to characterize the average distribution of the Hurst index in the directions of longitude and latitude (Table 3).

We performed integrated analysis based on the slope of the unary linear regression and the Hurst index. Specifically, the regions with significant change in surface albedo were classified into five categories. We fully revealed the past trend and future change of surface albedo based on the dimensionality reduction analysis in the direction of longitude (or latitude), as shown in Table 4.

Table 2 Three main forms of the Hurst index indicating the persistence status of time series

H	Persistence status of time series
0.50–1.00	Persistence series, i.e., future change is highly likely to be consistent with the past trend.
0.50	Random discrete series, i.e., the trend of future change is independent of the past trend.
0.00–0.50	Anti-persistence series, i.e., future change is most likely to show the opposite trend from the past trend.

Note: *H* is the Hurst index.

Table 3 Seven levels of the Hurst index indicating the persistence status of time series and their corresponding spatial distribution function values

H	Persistence status		Spatial distribution function value
0.00–0.20	Extremely strong anti-persistence	Significant anti-persistence	–1.00
0.20–0.25	Strong anti-persistence		–0.50
0.25–0.35	Stronger anti-persistence		–0.25
0.35–0.65	Weak anti-persistence or weak persistence		-
0.65–0.75	Stronger persistence	Significant persistence	0.25
0.75–0.80	Strong persistence		0.50
0.80–1.00	Extremely strong persistence		1.00

Note: "-" means no value.

Table 4 Integrated analysis on the past trend and future change of surface albedo based on the slope of the unary linear regression and the Hurst index

Slope	*H*	Integrated trend (past trend and future change)	Spatial distribution function value
>0.0000	>0.50	Trending up in the past, and continuing to rise in the future	1.00
>0.0000	<0.50	Trending up in the past, but trending the opposite way in the future	–1.00
<0.0000	>0.50	Trending down in the past, and continuing to decline in the future	1.00
<0.0000	<0.50	Trending down in the past, but trending the opposite way in the future	–1.00
-	0.50	Unchanged and discrete sequence	-

Note: Slope indicates the linear trend per decade. "-" means no value.

2.3.3 Correlation analysis

Pearson's correlation coefficient was used to reveal the relationship between average surface albedo (at the annual and seasonal scales) and influencing factors (NDSI, precipitation, NDVI, land surface temperature, soil moisture, and air temperature) in northern Xinjiang (Fig. 2c), and the significance *t*-test was conducted. The dimensionality reduction method was applied to analyze the spatial distribution of Pearson's correlation coefficients (Table 5). The formula is as follows:

$$R_{XY} = \frac{\sum_{i=1}^{n}(X_i - \bar{X})(Y_i - \bar{Y})}{\sqrt{\sum_{i=1}^{n}(X_i - \bar{X})^2 \sum_{i=1}^{n}(Y_i - \bar{Y})^2}}, \tag{8}$$

where R_{XY} is the correlation coefficient between variables X and Y; n is the total number of years;

X_i and Y_i are the values of variables X and Y in the i^{th} year (i=1, 2, ⋯, n), respectively; and $\overline{X}$ and $\overline{Y}$ are the mean values of variable X and Y over the study period.

Table 5 Classification criteria and spatial distribution function values for the correlation between surface albedo and each influencing factor

Correlation		Correlation coefficient	P	Spatial distribution function value
Significant positive correlation	Extreme positive correlation	>0.00	<0.01	1.00
	Intermediate positive correlation	>0.00	0.01–0.05	0.50
Significant negative correlation	Extreme negative correlation	<0.00	<0.01	–1.00
	Intermediate negative correlation	<0.00	0.01–0.05	–0.50

2.3.4 Influencing factor analysis

The RF model was used to measure the importance of influencing factors (NDSI, precipitation, NDVI, land surface temperature, soil moisture, air temperature, and DEM) on surface albedo. Both the factor detector and interaction detector in the Geodetector were used to reveal the influence and significance of each influencing factor on surface albedo, the strength of the interaction between influencing factors, and the influence of influencing factors interactively (Fig. 2c).

The RF model is considered a useful method to evaluate the importance of factors through model calculation (Liu et al., 2018; Gomes et al., 2019), and the ranking of the importance of factors obtained by this method is relatively unbiased and more accurate (Grömping, 2009). The model has two reliable metrics in calculating the importance of factors, i.e., the percentage increase in mean squared error (%IncMSE) and the average increase in node purity (IncNodePurity). In this study, IncNodePurity was used as a metric to assess the importance of each influencing factor on surface albedo. The larger the value, the more important the influencing factor.

The Geodetector is an effective method to test the single-factor spatial heterogeneity and multi-factor coupling. This study used the factor detection to analyze the spatial heterogeneity of surface albedo and the influence q of each influencing factor on the spatial heterogeneity of surface albedo. The value of q indicates that the influencing factor explains q×100% of the spatial heterogeneity of surface albedo (Wang and Xu, 2017). A larger value of q indicates a stronger explanatory power, and vice versa. The formula is as follows:

$$q = 1 - \frac{\sum_{h=1}^{L} N_h \sigma_h^2}{N\sigma^2} = 1 - \frac{SSW}{SST}, \tag{9}$$

where h is the stratification of surface albedo (or its influencing factors); N_h and N are the number of elements in stratum h (h=1, 2, ..., L) and the whole area, respectively; σ_h^2 and σ^2 are the variances of surface albedo in stratum h and the whole area, respectively; and SSW and SST are the sum of variance within a stratum and the total variance of the whole area, respectively.

In addition, $q(X_1 \cap X_2)$ (where X_1 is an influencing factor of surface albedo and X_2 is another influencing factor of surface albedo), which is the influence of the interaction of X_1 and X_2 on the spatial heterogeneity of surface albedo, was used to detect and identify whether the influence of interaction among different influencing factors on surface albedo was correlated or independent (Table 6).

The parameters in the Geodetector were optimized by optimizing the spatial discretization. Three discretization methods (i.e., equal, natural, and quantile) and a combination of 3–500 stratifications was used for each influencing factor to calculate the corresponding q value. From the perspective of spatial stratification heterogeneity, the combination of the discretization method

and stratification is the optimal parameter when the q value is maximum. We calculated seven influencing factors based on the GD package (Song et al., 2020) using the quantile discretization method. The stratification numbers of NDSI, precipitation, NDVI, land surface temperature, soil moisture, air temperature, and DEM were 478, 491, 478, 485, 498, 493, and 397, respectively.

Table 6 Influence criterion intervals and interaction types caused by the interaction between influencing factors

Interval	Interaction explanation
$q(X_1 \cap X_2) < \text{Min}[q(X_1), q(X_2)]$	Nonlinear weakening
$\text{Min}[q(X_1), q(X_2)] < q(X_1 \cap X_2) < \text{Max}[q(X_1), q(X_2)]$	Single-factor nonlinear weakening
$q(X_1 \cap X_2) > \text{Max}[q(X_1), q(X_2)]$	Dual factor enhancement
$q(X_1 \cap X_2) = q(X_1) + q(X_2)$	Independence
$q(X_1 \cap X_2) > q(X_1) + q(X_2)$	Nonlinear enhancement

Note: X_1 is an influencing factor of surface albedo; X_2 is another influencing factor of surface albedo; $q(X_1)$ and $q(X_2)$ are the influences of X_1 and X_2 on the spatial heterogeneity of surface albedo, respectively; $q(X_1 \cap X_2)$ is the influence of the interaction of X_1 and X_2 on the spatial heterogeneity of surface albedo. Min, minimum; Max, maximum.

3 Results

3.1 Spatial distribution patterns of surface albedo

The spatial distribution characteristics of the seasonal and annual average surface albedo in northern Xinjiang from 2010 to 2020 are shown in Figure 3. The annual average surface albedo from 2010 to 2020 in the study area ranged from 0.10 to 0.56, with a mean value of 0.28. The gray area map in Figure 3e clearly shows that the overall annual average surface albedo was high in the west and north, and low in the east and south. The eastern part of the study area was the center of low surface albedo values, mostly less than 0.20. In addition, the surface albedo values of lakes such as the Ulungur Lake and Ebinur Lake were also less than 0.20. Surface albedo values in the western part of the study area mostly ranged between 0.20 and 0.30. The values in most of the central region, such as the Junggar Basin, were greater than 0.30, especially in the northerly Altay Mountains (reaching 0.56), which was the center of high surface albedo values in the study area.

The spatial distribution of the seasonal average surface albedo was similar to that of the annual average surface albedo (Fig. 3a–d), i.e., high in the west and low in the east. However, in spring, summer, and autumn, the seasonal average surface albedo decreased first and then increased from north to south. In winter, it was obviously different, that is, the seasonal average surface albedo was higher than 0.40 in most areas of the central and western regions, and mostly less than 0.30 in the eastern region. In addition, the seasonal average surface albedo in winter first increased and then decreased from north to south, with the highest average value of 0.42 (Fig. 3d). In spring, the average surface albedo was significantly lower, with an average value of 0.28 (Fig. 3a), and the spatial distribution of the seasonal average surface albedo in spring was extremely similar to that of the annual average surface albedo. In summer, the average surface albedo decreased to the lowest value of 0.19 (Fig. 3b), and the values of lakes such as the Ulungur Lake and Ebinur Lake were less than 0.10. The average surface albedo in autumn was 0.25, which was higher than that in summer but slightly lower than that in spring (Fig. 3c).

3.2 Spatiotemporal variation characteristics of surface albedo and its influencing factors

3.2.1 Temporal variation

The inter-annual variation of surface albedo generally showed a decreasing trend with a slope of –0.0069/10a from 2010 to 2020 (Fig. 4). However, the performance was different in different seasons. In spring, the greatest decreasing rate of surface albedo was –0.0348/10a; in summer, it showed a weak decreasing trend at a rate of –0.0041/10a; and in autumn and winter, it showed an increasing trend at rates of 0.0120/10a and 0.0156/10a, respectively. The results of the annual and seasonal average surface albedo did not reach the significance level (P>0.05), indicating that the variation trend of surface albedo was not significant. In terms of the influencing factors of surface

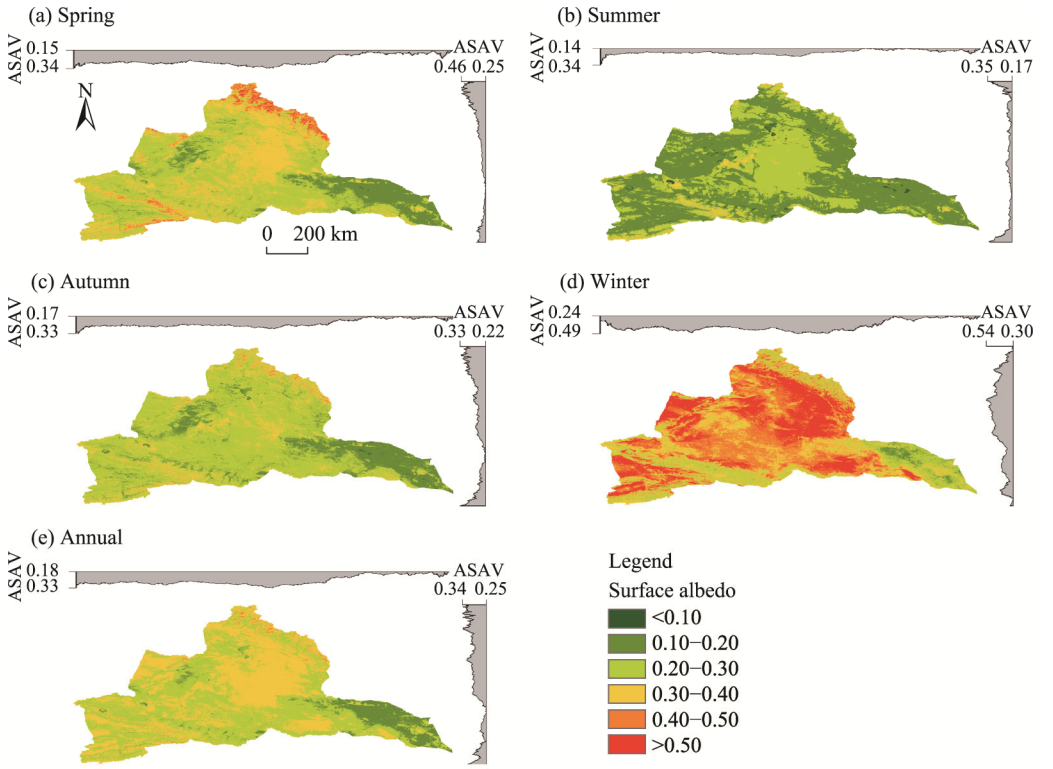

Fig. 3 Spatial distribution characteristics of the seasonal average surface albedo (a–d) and annual average surface albedo (e) from 2010 to 2020. The gray area maps show the average surface albedo values in the longitudinal and latitudinal directions. Note that the figures are based on the standard map (GS (2019) 1822) from the Standard Map Service System (http://bzdt.ch.mnr.gov.cn/index.html), and the standard map has not been modified. ASAV, average surface albedo value.

albedo at the annual scale, NDSI and precipitation showed a decreasing trend, while NDVI, land surface temperature, soil moisture, and air temperature all exhibited an increasing trend. In spring, NDSI significantly decreased, while air temperature and NDVI significantly increased. In addition, soil moisture significantly increased in winter.

3.2.2 Spatial variation

The annual and seasonal average surface albedo from 2010 to 2020 showed large spatial variations (Fig. 5). During the study period, the annual average surface albedo decreased mainly in the south of the study area and increased in some northern regions (Fig. 5e). The area showing significant decrease of surface albedo was about 8.77×10^3 km^2 (1.95% of the study area), and the area showing significant increase of surface albedo was about 16.67×10^3 km^2 (3.71% of the study area) (Fig. 5f). The seasonal average surface albedo had similar spatial distributions as the annual average surface albedo, but contributed unevenly to the long-term variation of the annual average surface albedo (Fig. 5a and b). Significant decreases of surface albedo were observed in more than 5.90% of the study area in both spring and summer, obviously higher than the area proportion of regions with significant increase of surface albedo; however, the condition was opposite in autumn and winter, which was consistent with the overall trend shown in Figure 4. Land cover types had a significant impact on the change in surface albedo; specifically, among different land cover types, the largest area proportion of regions showing significant decrease of surface albedo was cropland in spring (9.37% of the study area) and impervious surface in summer (14.37% of the study area), whereas the largest area proportion of regions showing significant increase of surface albedo was water bodies in autumn (11.56% of the study area) and bare land in winter (14.37% of the study area) (Fig. 5f).

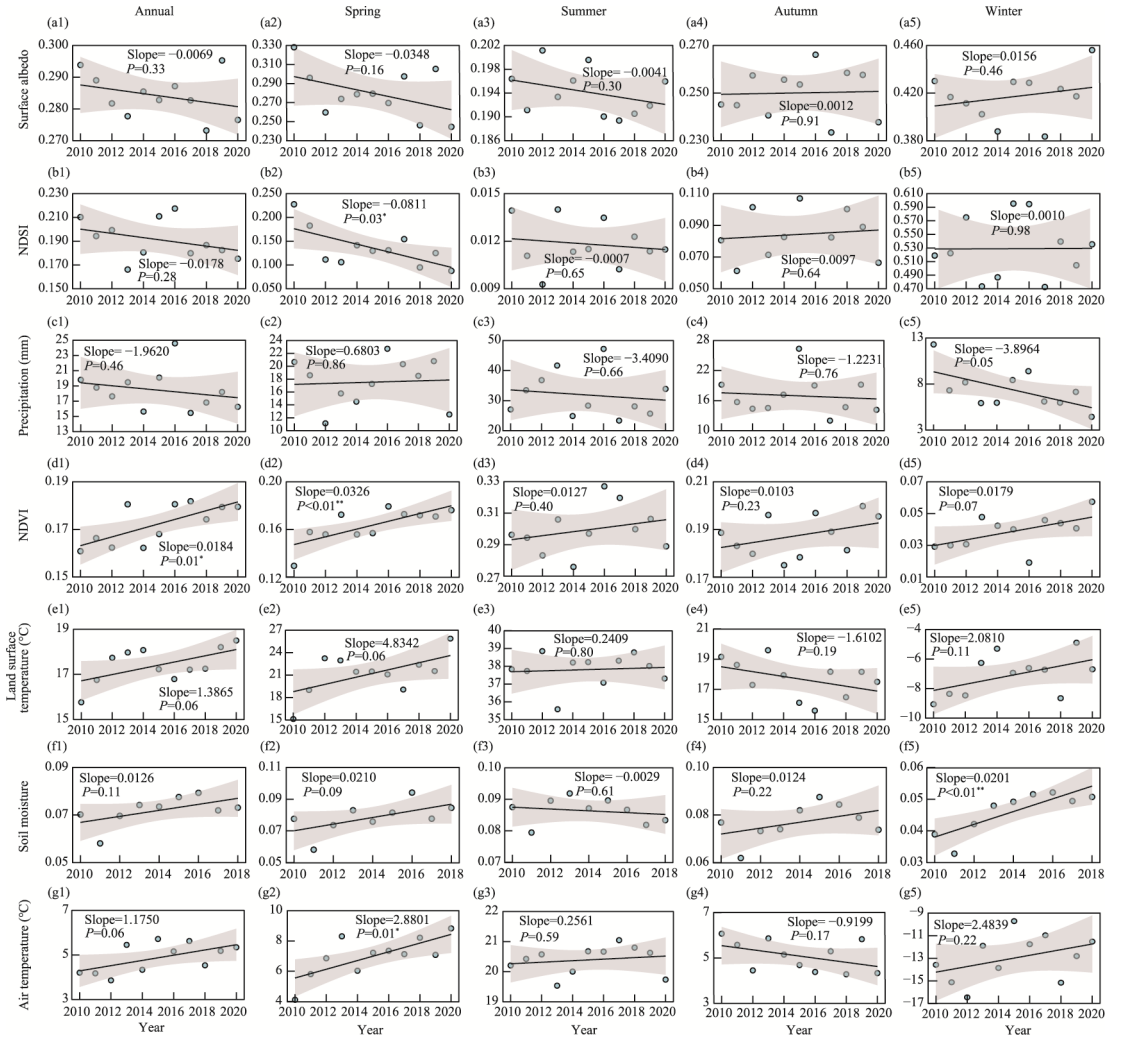

Fig. 4 Temporal variations of the annual and seasonal average surface albedo and its influencing factors from 2010 to 2020. (a1–a5), surface albedo; (b1–b5), NDSI; (c1–c5), precipitation; (d1–d5), NDVI; (e1–e5), land surface temperature; (f1–f5), soil moisture; (g1–g5), air temperature. Blue circles are data values, black lines are trend lines, and gray areas are 95% confidence intervals. Slope indicates the linear trend per decade. **, $P<0.01$ level; *, $P<0.05$ level.

3.2.3 Trend analysis

As shown in Figure 6, the persistence status of the annual and seasonal average surface albedo during the study period also showed some spatial variations. More regions exhibited significant persistence (14.79% of the study area) and fewer regions indicated significant anti-persistence (6.63% of the study area) at the annual scale. There were more regions showing significant persistence of the seasonal average surface albedo in spring and summer (15.78% and 20.28% of the study area, respectively) than the regions showing significant anti-persistence (7.30% and 3.89% of the study area, respectively) (Fig. 6a and b), especially in summer. The area proportions of regions showing significant persistence of the seasonal average surface albedo in autumn and winter (9.27% and 13.27% of the study area, respectively) were close to the area proportions of regions showing significant anti-persistence in these two seasons (11.05% and 7.65% of the study area, respectively) (Fig. 6c and d). The persistence status of surface albedo of different land cover types was similar to that of the overall study area (Fig. 6f).

The slope of the unary linear regression and Hurst index calculated above were used to analyze the integrated variation trend of surface albedo in the study area (Fig. 7). According to the results,

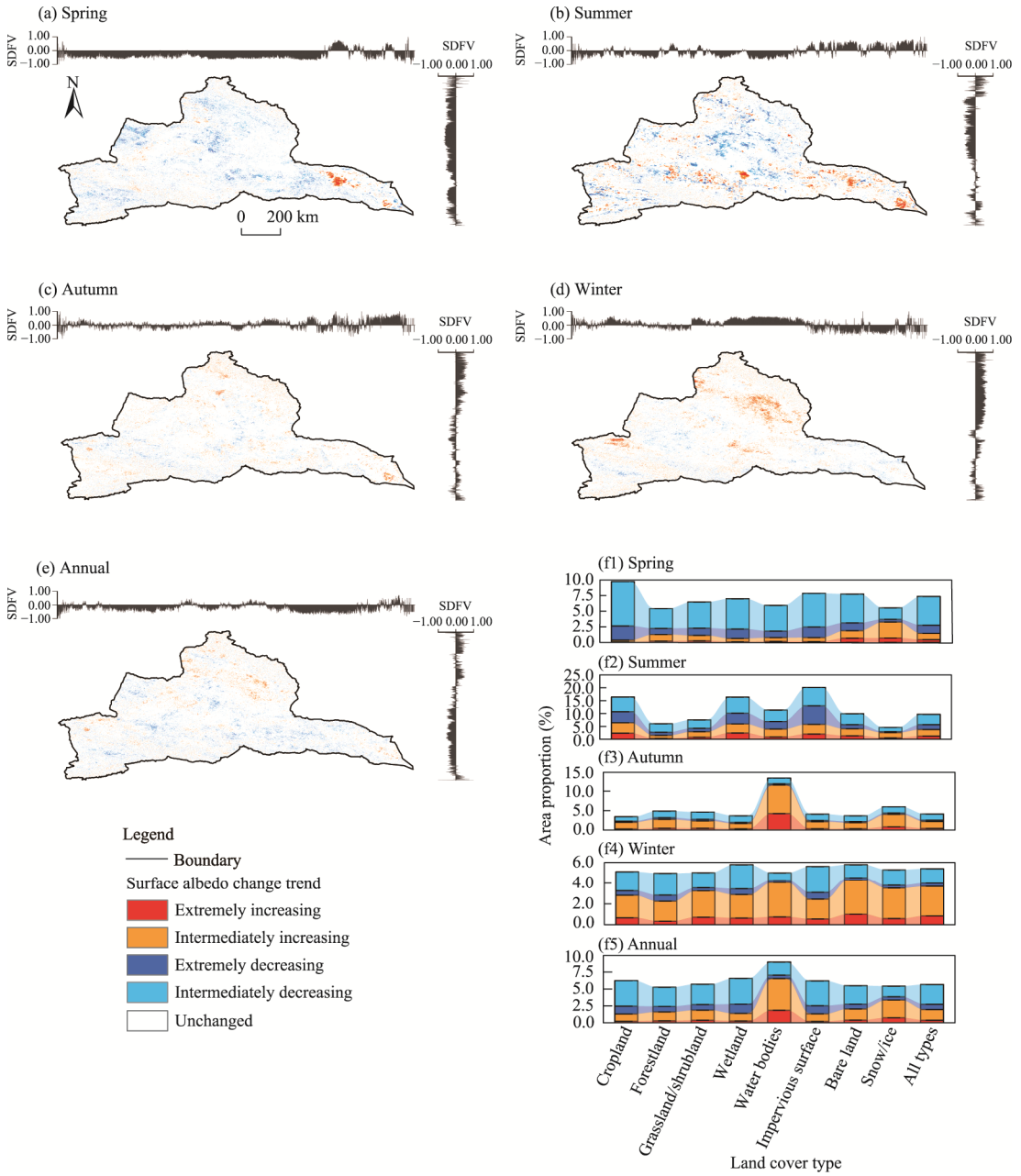

Fig. 5 Spatial distribution characteristics of the variation trends of the annual and seasonal average surface albedo (a–e) and their area proportions in different land cover types (except for the area proportion of regions with unchanged trend of surface albedo; f1–f5) from 2010 to 2020. The gray area maps show the spatial distribution function values (the closer the spatial distribution function value is to 1.00, the more significantly the surface albedo increases; and the closer the value to –1.00, the more significantly the surface albedo decreases; see Table 1 for details) of the variation trends of surface albedo in the latitudinal and longitudinal directions. The semitransparent color band between histograms represents the change of area proportion in adjacent land cover types. Note that the figures are based on the standard map (GS (2019) 1822) from the Standard Map Service System (http://bzdt.ch.mnr.gov.cn/index.html), and the standard map has not been modified. SDFV, spatial distribution function value.

the average surface albedo in 1.08% of the study area showed trending up in the past, and continuing to rise in the future (slope>0.00 and Hurst index>0.50); the average surface albedo in 2.12% of the study area showed trending down in the past, and continuing to decline in the future

(slope<0.00 and Hurst index>0.50); the average surface albedo in 1.59% of the study area showed trending down in the past, but trending the opposite way in the future (slope<0.00 and Hurst index<0.50); and the average surface albedo in 0.87% of the study area showed trending up in the past, but trending the opposite way in the future (slope>0.00 and Hurst index<0.50). Among the regions with significant change in the annual average surface albedo, the area proportion of regions

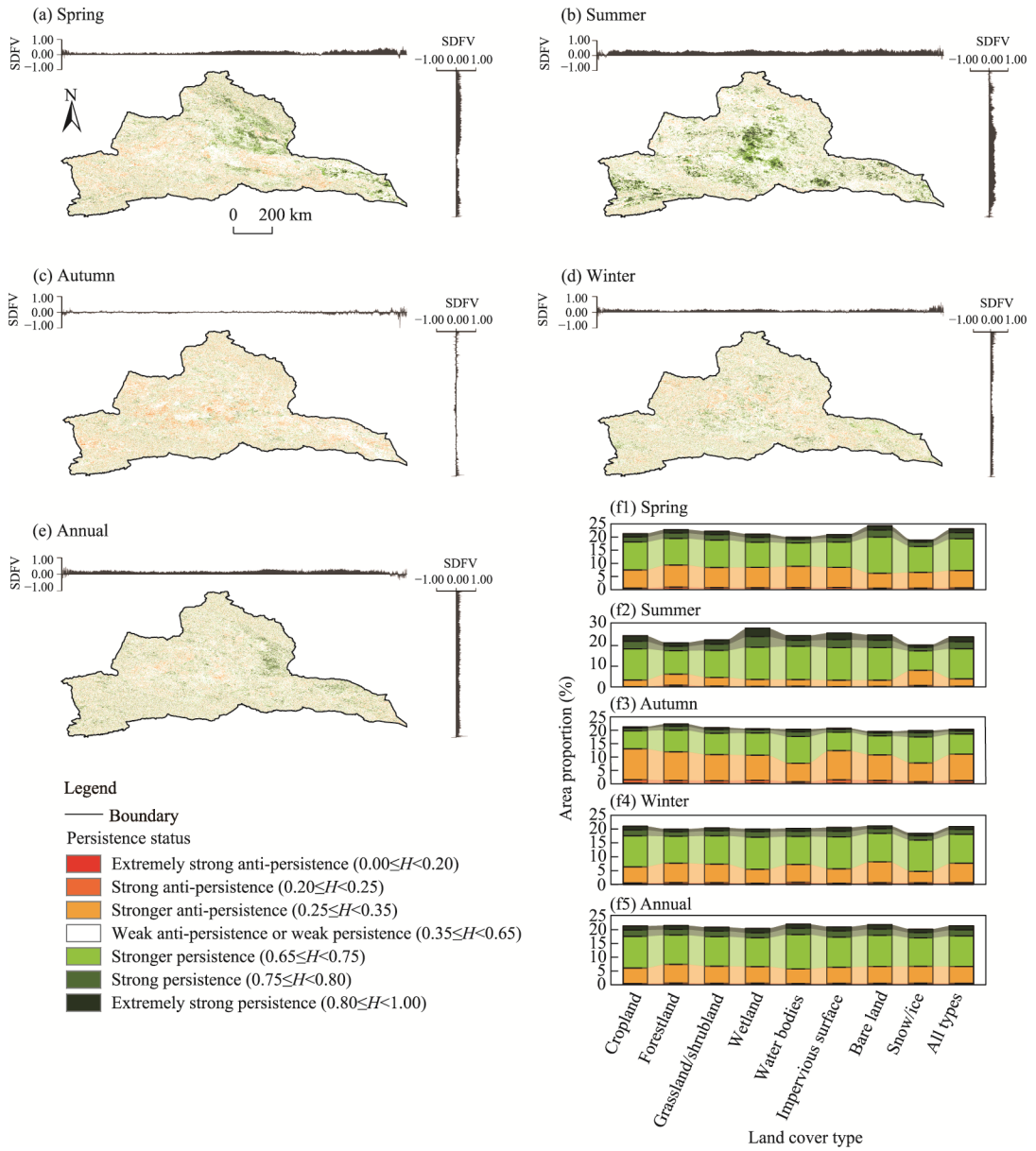

Fig. 6 Spatial distribution characteristics of the persistence status of the annual and seasonal average surface albedo (a–e) and their area proportions in different land cover types (except for the area proportion of regions with weak anti-persistence or weak persistence of surface albedo; f1–f5) from 2010 to 2020. The gray area maps show the spatial distribution function values (the closer the spatial distribution function value to 1.00, the stronger the persistence, and the closer the value to –1.00, the stronger the anti-persistence; see Table 3 for details) of the persistence status of surface albedo in the latitudinal and longitudinal directions. The semitransparent color band between histograms represents the change of area proportion in adjacent land types. Note that the figures are based on the standard map (GS (2019) 1822) from the Standard Map Service System (http://bzdt.ch.mnr.gov.cn/index.html), and the standard map has not been modified. SDFV, spatial distribution function value.

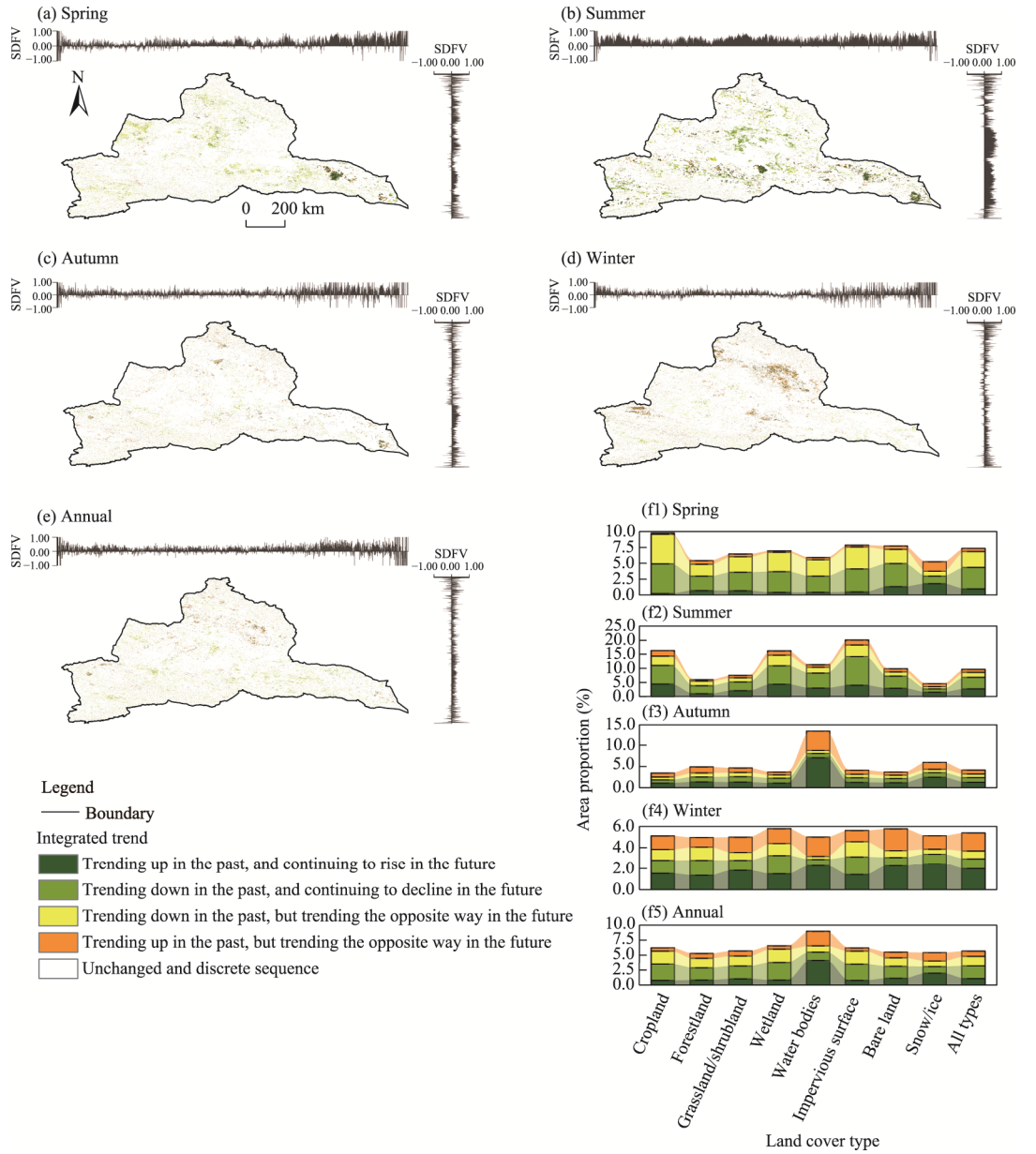

Fig. 7 Spatial distribution characteristics of the integrated trends of the annual and seasonal average surface albedo (a–e) and their area proportions in different land cover types (except for the area proportion of regions with unchanged and discrete sequence of surface albedo; f1–f5) from 2010 to 2020. The gray area maps show the spatial distribution function values (the closer the spatial distribution function value to 1.00, the more similar in the change trend of surface albedo between the past and future, and the closer the spatial distribution function value to –1.00, the more opposite in the change trend of surface albedo between the past and future; see Table 4 for details) of integrated trends in the latitudinal and longitudinal directions. The semitransparent color band between histograms represents the change of area proportion in adjacent land types. Note that the figures are based on the standard map (GS (2019) 1822) from the Standard Map Service System (http://bzdt.ch.mnr.gov.cn/ index.html), and the standard map has not been modified. SDFV, spatial distribution function value.

showing the same trend in the past and future (3.20% of the study area) was significantly higher than that of regions showing the opposite trend (2.46% of the study area) (Fig. 7e). In addition, the area proportion of regions showing an increasing (2.67% of the study area) or decreasing (2.99% of the study area) trend in the future was similar.

The integrated trend of the seasonal average surface albedo was similar to that of the annual

average surface albedo. Among the regions with significant seasonal variations, the area proportions of regions showing the same trend in the past and future (spring: 4.34% of the study area; summer: 6.83% of the study area; autumn: 2.37% of the study area; winter: 2.94% of the study area) were much greater than those of regions showing the opposite trend in the past and future (spring: 3.00% of the study area; summer: 2.81% of the study area; autumn: 1.77% of the study area; winter: 2.44% of the study area) (Fig. 7a–d). In addition, the area proportions of regions showing the upward and downward trends in the future were also similar. For certain land cover types, the area proportion of regions showing a decreasing trend of surface albedo in the past clearly shifted to an increasing trend in the future to a large scale. For instance, the surface albedo of cropland in spring and impervious surface in summer shifted from a decreasing trend in the past to an increasing trend in the future in 4.68% and 4.12% of the study area, respectively. Meanwhile, a large area of regions shifted from an increasing trend of surface albedo in the past to a decreasing trend in the future, such as water bodies in autumn (4.68% of the study area) and bare land in winter (2.05% of the study area) (Fig. 7f).

3.3 Influencing factors of surface albedo

3.3.1 Correlation analysis results

The relationship between the annual average surface albedo and various influencing factors during the study period showed strong spatial heterogeneity (Fig. 8). The regions where surface albedo was significantly positively correlated with NDSI and precipitation accounted for 95.37% and 2.40% of the study area, respectively. Among them, surface albedo was extremely positively correlated with NDSI in bare land (in 90.89% of the bare land area) and all other land cover types (in more than 99.00% of each land cover type area) (Fig. 8g). Only some bare land regions in the eastern part of the study area showed no significant correlation between surface albedo and NDSI (Fig. 8a). The regions where surface albedo was significantly negatively correlated with precipitation accounted for 1.84% of the study area, with only a few patches showing extreme negative correlation (0.31% of the study area) or intermediate negative correlation (1.53% of the study area). The regions showing extreme positive correlation between surface albedo and precipitation were scattered throughout the study area (Fig. 8b), in which wetland accounted for the highest area proportion among all land cover types, with surface albedo in 3.23% of wetland significantly positively correlated with precipitation (Fig. 8g).

Surface albedo was mainly negatively correlated with NDVI, land surface temperature, soil moisture, and air temperature (Fig. 8c–f), and regions with significant negative correlations accounted for 4.54%, 7.41%, 3.65%, and 3.14% of the study area, respectively. Specifically, regions showing extreme negative correlations of surface albedo with NDVI, land surface temperature, soil moisture, and air temperature accounted for 1.06%, 2.00%, 0.80%, and 0.64% of the study area, respectively; whereas regions with intermediate negative correlations accounted for 3.48%, 5.41%, 2.86%, and 2.51% of the study area, respectively. Regions with significant positive correlations of surface albedo with NDVI, land surface temperature, soil moisture, and air temperature accounted for 1.49%, 1.08%, 1.79%, and 1.62% of the study area, respectively. Specifically, for these four influencing factors, only a few patches showed extreme positive correlations (0.29%, 0.20%, 0.32%, and 0.29% of the study area, respectively) or intermediate positive correlations (1.20%, 0.87%, 1.46%, and 1.32% of the study area, respectively). The area proportions of regions where surface albedo was significantly negatively correlated with NDVI (6.19% of the study area), soil moisture (5.04% of the study area), and air temperature (5.34% of the study area) were higher in cropland than in other land cover types, and the area proportion of regions with a significant negative correlation between surface albedo and land surface temperature was the highest in bare land (Fig. 8g).

The correlations between surface albedo and each influencing factor showed significant seasonal differences (Fig. 9). The correlation between surface albedo and NDSI was most obvious in winter, with a significant positive correlation in 93.27% of the study area, followed by spring (62.23% of the study area) and autumn (53.56% of the study area). However, in summer, because

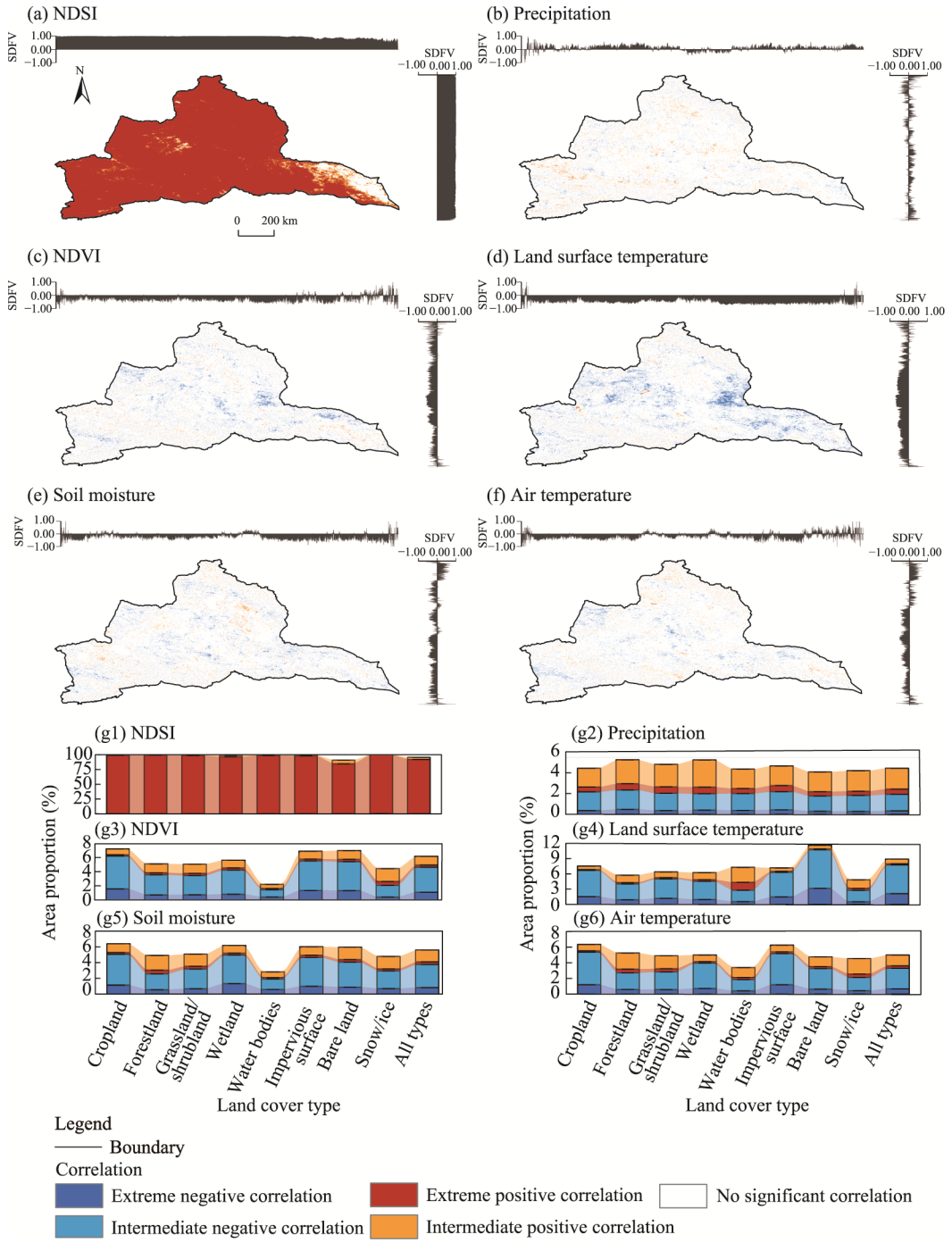

Fig. 8 Spatial distribution characteristics of correlations between the annual average surface albedo and influencing factors (a–f) and their area proportions in different land cover types (except for the area proportion of regions with no significant correlation; g1–g6) from 2010 to 2020. The gray area maps show the spatial distribution function values (the closer the spatial distribution function value to 1.00, the more significant positive correlation between the annual average surface albedo and influencing factor, and the closer the spatial distribution function value to –1.00, the more significant negative correlation between the annual average surface albedo and influencing factor; see Table 5 for details) of correlations in the latitudinal and longitudinal directions. The semitransparent color band between histograms represents the change of area proportion in adjacent land types. Note that the figures are based on the standard map (GS (2019) 1822) from the Standard Map Service System (http://bzdt.ch.mnr.gov.cn/index.html), and the standard map has not been modified. SDFV, spatial distribution function value.

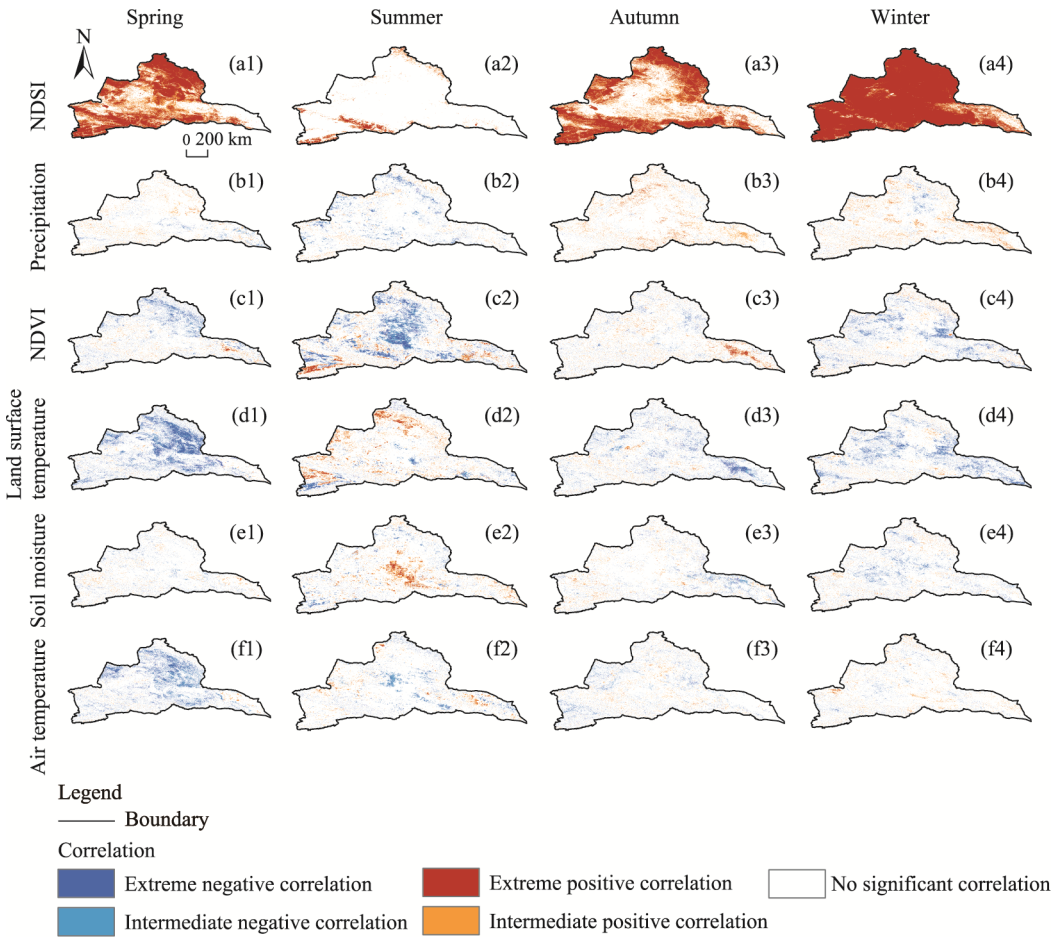

Fig. 9 Spatial distribution characteristics of correlations between the seasonal average surface albedo and influencing factors from 2010 to 2020. (a1–a4), NDSI; (b1–b4), precipitation; (c1–c4), NDVI; (d1–d4), land surface temperature; (e1–e4), soil moisture; (f1–f4), air temperature. Note that the figures are based on the standard map (GS (2019) 1822) from the Standard Map Service System (http://bzdt.ch.mnr.gov.cn/index.html), and the standard map has not been modified.

snow melted out in most regions and only a few high-altitude regions still had snow, the significant correlation between surface albedo and NDSI was not available in most regions, and only 5.41% of the study area showed a significant positive correlation, while 88.69% of the snow- and ice-covered regions showed a significant positive correlation. In autumn and winter, regions with a significant positive correlation between surface albedo and precipitation accounted for 4.55% and 4.39% of the study area, respectively, which were obviously higher than the area proportions of regions with a significant negative correlation (0.78% and 2.08% of the study area, respectively). The correlations between surface albedo and precipitation showed small differences among spring, autumn, and winter, whereas the distribution was the opposite in summer. There were significantly less regions with a significant positive correlation (1.30% of the study area) than those with a significant negative correlation (4.58% of the study area) in summer. For NDVI, land surface temperature, soil moisture, and air temperature, extreme negative correlations were dominant in almost all seasons, except for significant positive correlations between surface albedo and land surface temperature and between surface albedo and soil moisture in summer, as well as significant positive correlation between surface albedo and NDVI in autumn.

3.3.2 Importance analysis results

The RF model was used to assess the importance of each influencing factor on surface albedo

during the study period. The RF model explained 67.89% of the average surface albedo from 2010 to 2018, and the two metric index values of %IncMSE and IncNodePurity are shown in Table 7. In this study, IncNodePurity was selected as the importance index, and the overall importance of each influencing factor on the average surface albedo from 2010 to 2018 can be ranked as: NDSI (IncNodePurity of 1.75)>precipitation (0.89)>land surface temperature (0.81)>soil moisture (0.73)>DEM (0.61)>NDVI (0.46)>air temperature (0.42).

Table 7 Importance analysis of each influencing factor on the average surface albedo from 2010 to 2018 based on the random forest model

Influencing factor	%IncMSE (%)	IncNodePurity
NDSI	65.30	1.75
Precipitation	38.77	0.89
Land surface temperature	34.61	0.81
Soil moisture	46.31	0.73
DEM	52.58	0.61
NDVI	36.31	0.46
Air temperature	34.85	0.42

Note: NDSI, Normalized Difference Snow Index; DEM, digital elevation model; NDVI, Normalized Difference Vegetation Index; %IncMSE, the percentage increase in mean squared error; IncNodePurity, the average increase in node purity.

Using the above method, the importance of each influencing factor on surface albedo was evaluated annually from 2010 to 2018 (Fig. 10). In these years, the mean value of IncNodePurity for each influencing factor can be ranked as: NDSI (2.42)>precipitation (1.52)>soil moisture (1.39)>land surface temperature (1.36)>DEM (1.12)>air temperature (0.98)>NDVI (0.96) (Fig. 10a), indicating that NDSI, land surface temperature, precipitation, and soil moisture were the dominant influencing factors over the years, while DEM, NDVI, and air temperature had relatively weak influences on surface albedo. In addition, the influence degree of each influencing factor on surface albedo fluctuated over the years. For example, the influence degrees of NDSI on surface albedo in 2012 (IncNodePurity of 3.00) and 2014 (IncNodePurity of 2.88) were much higher than the average IncNodePurity (2.42) of NDSI during 2010–2018 (Fig. 10b).

In order to further test the influencing factors of surface albedo, we used the factor detector and interaction detector to quantitatively assess the impact of each influencing factor alone and in interactive combination on surface albedo. Firstly, the q-value of each influencing factor in the study area was calculated and analyzed using the factor detector (Fig. 11a), and the results showed that the impact of each influencing factor on surface albedo in the study area was ranked as: NDSI (q-value of 0.622)>precipitation (0.516)>land surface temperature (0.486)>soil moisture (0.454)>NDVI (0.396)>air temperature (0.327)>DEM (0.236). Only DEM had an insignificant influence on surface albedo, while the other influencing factors all met the 99% of confidence interval (P<0.01). The spatial variation of surface albedo was caused by the combined effect of various influencing factors, among which NDSI had the greatest contribution, and precipitation, land surface temperature, and soil moisture also had great contributions. The q-values of these factors were all greater than 0.400. In contrast, the contributions of NDVI, air temperature, and DEM were relatively small, with the q-value of 0.236 on average. These results were highly consistent with the findings obtained from the RF model, which confirmed that NDSI was the primary influencing factor of surface albedo, and precipitation, land surface temperature, and soil moisture also showed strong influence on surface albedo, while NDVI, air temperature, and DEM had relatively small influences on surface albedo.

The interaction between influencing factors and their influence on the spatial variation of surface albedo were analyzed using the interaction detector (Fig. 11b). The results showed that the effect of the interaction of any two influencing factors on surface albedo was greater than that of a single influencing factor, indicating a dual factor enhancement or nonlinear enhancement effect.

Among them, both air temperature and DEM showed a nonlinear enhancement with the other four influencing factors (NDSI, precipitation, land surface temperature, and soil moisture). This indicated that although the single influencing factor of air temperature and DEM had little effects on surface albedo, their influences could be significantly improved by interacting with other factors, and their *q*-values were mostly greater than those of the two single influencing factors. In addition, NDVI showed a nonlinear enhancement under the interaction with land surface temperature or precipitation, with an explanatory power for the spatial heterogeneity of surface albedo greater than 92.00%. The interaction of other influencing factors also showed different degrees of enhancement, and the explanatory power for the spatial heterogeneity of surface albedo exceeded 57.70%.

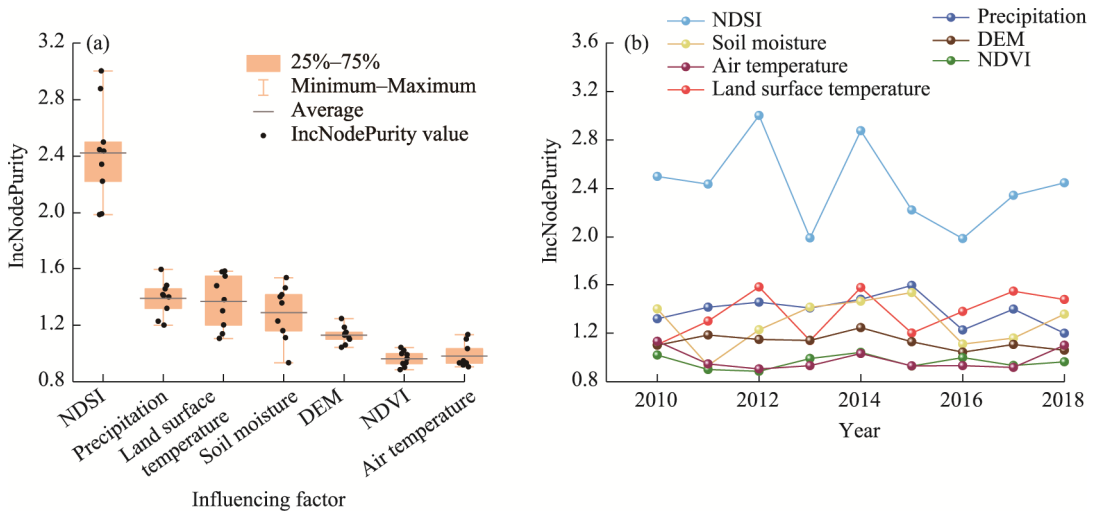

Fig. 10 Box-plot (a) and line chart (b) of the IncNodePurity values for each influencing factor of surface albedo from 2010 to 2018. IncNodePurity, the average increase in node purity.

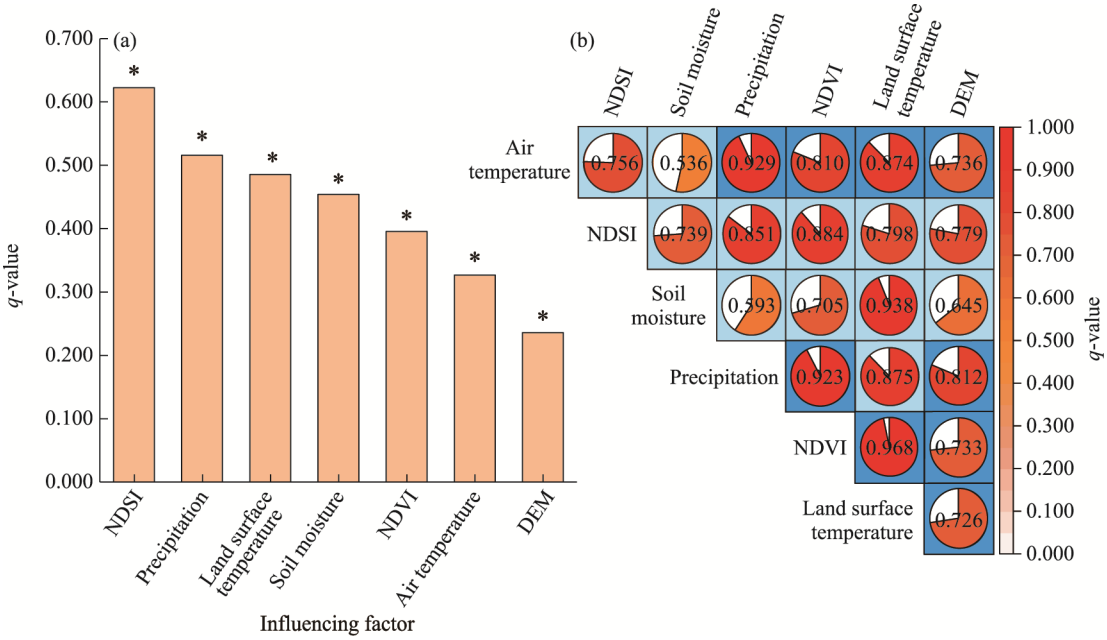

Fig. 11 Results of factor detector (a) and interaction detector (b) in Geodetector analysis showing the impact of each influencing factor on surface albedo. *, 99% of confidence interval (P<0.01). Dark blue and light blue represent the two-factor interaction with nonlinear enhancement and dual factor enhancement, respectively. Values in the circles indicate the *q*-values.

4 Discussion

4.1 Influence mechanisms of surface albedo

Surface albedo is directly or indirectly affected by factors such as NDSI, NDVI, soil moisture, land surface temperature, precipitation, and air temperature (Wielicki et al., 2005; Gorelick et al., 2017). Among them, changes in factors related to soil properties (e.g., soil moisture) and surface cover (e.g., NDSI and NDVI) directly affect surface albedo (Kala et al., 2014). In the context of global warming, snow is an extremely important and rapidly changing element, especially in northern Xinjiang (Bormann et al., 2018). Because the surface albedo of snow varies with the change of snow, for instance, 0.90 of fresh snow, 0.40 of melting snow, and 0.20 of polluted snow (Moody et al., 2007), the contribution of the change of snow to surface albedo is greater than other factors (Figs. 10 and 11). The shading effect of vegetation on snow significantly reduces surface albedo (Loranty et al., 2014), and change in NDVI can also alter the surface albedo in snow-free regions due to the optical contrast between vegetation canopy and underlying soil surface (Alessandri et al., 2017). When the soil varies from dry to wet, its color becomes dark, enhancing the ability of soil surface to absorb light (Gascoin et al., 2009). Compared with the surface albedo of above 0.70 of the dry soil, the moist soil has a lower surface albedo of less than 0.50 (Alessandri et al., 2021). Therefore, increasing soil moisture will reduce surface albedo and increase net radiation and evaporation rate.

In addition, land surface temperature, precipitation, and air temperature can also affect surface albedo through different mechanisms, such as the influences of NDSI, NDVI, and soil moisture (Alibakhshi et al., 2019). To further understand the effects of these factors on surface albedo, this study evaluated the interaction between them. The change in land surface temperature can affect vegetation growth, which in turn influences the absorption of solar radiation through photosynthesis, leading to the variation in surface albedo (Zhao et al., 2014). This is consistent with the results in this study, that is, the interaction between land surface temperature and NDVI showed a nonlinear enhancement and had the highest explanatory power for the spatial heterogeneity of surface albedo (96.76%). Previous studies have revealed that meteorological factors, such as air temperature and precipitation, indirectly affect surface albedo by directly influencing other factors (e.g., Kala et al., 2014). For example, air temperature and precipitation can indirectly affect surface albedo by influencing vegetation growth (both air temperature and precipitation show a nonlinear enhancement effect on NDVI's effect on surface albedo), and the change in precipitation can alter the characteristics of snow, thus indirectly affecting surface albedo (the explanatory power of precipitation on the spatial heterogeneity of surface albedo is 85.15%, which is greater than that of NDVI). These conclusions are conducive to further understanding the feedback relationship in the land-atmosphere interaction process and provide scientific references and basis for verifying and improving land-surface process simulations (Li et al., 2020).

4.2 Attribution of the spatiotemporal variation in surface albedo

In this study, we found that the annual average surface albedo in northern Xinjiang showed a weak decreasing trend (Fig. 4), which was consistent with the slow decreasing trend of the annual average surface albedo in China's regional areas in recent years (Xu et al., 2020). In the other areas of the Northern Hemisphere, such as high-latitude regions (Loranty et al., 2014), the Arctic (Pistone et al., 2014), France (Planque et al., 2017), the Swiss Alps (Rangwala and Miller, 2012), and Greenland (He et al., 2013), the annual average surface albedo also shows a decreasing trend. The decreases in NDSI and precipitation, as well as the increases in NDVI, land surface temperature, soil moisture, and air temperature, jointly contributed to the decrease in surface albedo in northern Xinjiang. Among them, the contribution of change in NDSI to the variation in surface albedo was significantly higher than the contributions of other influencing factors (Pang et al., 2022). The decrease in NDSI was the main reason for the decrease in surface albedo, especially in spring. The interaction between land surface temperature and NDVI showed a

nonlinear enhancement, and the increase in land surface temperature affected vegetation growth, leading to a significant increase in NDVI. Similarly, land surface temperature increased most rapidly in spring, affecting vegetation growth and leading to the fastest increase in NDVI.

At the same time, climate change had a significant contribution to the decrease in surface albedo. Against the backdrop of warming temperature and reduced precipitation in northern Xinjiang from 2010 to 2020 (Fig. 4), the warming trend has promoted the expansion of vegetation (Pearson et al., 2013) and the melting of snow (Atlaskina et al., 2015), which reduced the high surface albedo of snow and increased the low surface albedo of vegetation. Meanwhile, the reduced snowfall and rainfall led to a decrease in NDSI, resulting in a decrease in surface albedo (Fassnacht et al., 2016; Malmros et al., 2018). In spring, the opposite trend of increasing rainfall resulted in an increase in soil moisture, which also caused a decrease in surface albedo in regions without snow and with sparse vegetation.

Among all land cover types, cropland in spring and impervious surface in summer contributed significantly to the decrease in surface albedo, and the area proportions of regions showing significant decrease in surface albedo occupied 9.37% and 14.37% of the study area, respectively, which were higher than the average area proportion of all land cover types in spring and summer (7.36% and 9.69% of the study area, respectively) (Fig. 5f). The area proportion of cropland where surface albedo showed extreme negative correlations with NDVI (6.19% of the study area) and soil moisture (5.04% of the study area) was the highest among all land cover types. This is due to that planting and irrigating crops will lead to a decrease in surface albedo by increasing NDVI and soil moisture, while impervious surface will disrupt the surface heat balance, resulting in significant warming in summer and subsequent decrease in surface albedo (Xu, 2009). Therefore, human activities have contributed to the decrease in surface albedo in northern Xinjiang, which indicates that more solar radiation will be absorbed, and thus warming will be accelerated in this area.

5 Conclusions

This study analyzed the spatial distribution and spatiotemporal variation characteristics of surface albedo in northern Xinjiang, as well as its responses to multiple influencing factors. The following conclusions were obtained.

(1) Surface albedo in the study area had obvious spatial and seasonal differences. The annual average surface albedo showed a spatial distribution pattern of high in the west and north and low in the east and south. The highest seasonal average surface albedo value occurred in winter while the lowest value was found in summer.

(2) During 2010–2020, the annual average surface albedo in the study area showed a weak decreasing trend. The spatial distribution of regions with significant change showed an increase in the north and a decrease in the south, and the area of regions with significant persistence was larger than that with significant anti-persistence. The trend and persistence status of the seasonal average surface albedo in spring and summer were similar to those of the annual average surface albedo, while the trend and persistence status of the seasonal average surface albedo in autumn and winter were opposite to those of the annual average surface albedo. The changing trend of surface albedo was generally stable and persistent, and land cover types had a significant influence on the variation of surface albedo. In addition, NDSI and precipitation showed a decreasing trend during the study period, while NDVI, land surface temperature, soil moisture, and air temperature showed an increasing trend.

(3) The annual average surface albedo was significantly positively correlated with NDSI and precipitation in many regions, and was mainly negatively correlated with NDVI, land surface temperature, soil moisture, and air temperature. In addition, the correlation between surface albedo and each influencing factor showed significant seasonal differences. Specifically, NDSI was the primary influencing factor of surface albedo, followed by precipitation, land surface temperature, and soil moisture, while NDVI, air temperature, and DEM had relatively small

influences. All influencing factors showed different degrees of enhancement in the interaction, especially air temperature and DEM. NDVI showed a nonlinear enhancement under the interaction with land surface temperature or precipitation.

The findings of this research can significantly enhance our understanding on the variation of surface albedo and its responses to various influencing factors. This research holds an immense importance in accurately comprehending the complex land-atmosphere interactions in northern Xinjiang, which can greatly improve the regional land-surface process simulation and climate prediction.

Conflict of interest

The authors declare that they have no known competing financial interests or personal relationships that could have appeared to influence the work reported in this paper.

Acknowledgements

This research was supported by the National Key Research and Development Program of China (2019YFC1510505), the Xinjiang University PhD Start-up Fund (BS210226), and the National College Student Research Training Plan of China (202210755004).

Author contributions

Conceptualization: YUAN Shuai, LIU Yongqiang, QIN Yan, ZHANG Kun; Methodology: YUAN Shuai, LIU Yongqiang; Formal analysis: YUAN Shuai, LIU Yongqiang; Data curation: YUAN Shuai, LIU Yongqiang; Writing - original draft preparation: YUAN Shuai; Writing - review and editing: YUAN Shuai, LIU Yongqiang; Funding acquisition: YUAN Shuai, LIU Yongqiang, QIN Yan; Resources: YUAN Shuai, LIU Yongqiang, QIN Yan, ZHANG Kun; Supervision: LIU Yongqiang; Visualization: YUAN Shuai; Investigation: YUAN Shuai, LIU Yongqiang, QIN Yan, ZHANG Kun; Validation: YUAN Shuai, LIU Yongqiang, QIN Yan, ZHANG Kun; Software: YUAN Shuai; Project administration: LIU Yongqiang.

References

Alessandri A, Catalano F, De Felice M, et al. 2017. Multi-scale enhancement of climate prediction over land by increasing the model sensitivity to vegetation variability in EC-Earth. Climate Dynamics, 49(4): 1215–1237.

Alessandri A, Catalano F, De Felice M, et al. 2021. Varying snow and vegetation signatures of surface-albedo feedback on the Northern Hemisphere land warming. Environmental Research Letters, 16(3): 034023, doi: 10.1088/1748-9326/abd65f.

Alibakhshi S, Hovi A, Rautiainen M. 2019. Temporal dynamics of albedo and climate in the sparse forests of Zagros. Science of the Total Environment, 663: 596–609.

Atlaskina K, Berninger F, de Leeuw G. 2015. Satellite observations of changes in snow-covered land surface albedo during spring in the Northern Hemisphere. The Cryosphere, 9(5): 1879–1893.

Bonan G B. 2008. Forests and climate change: forcings, feedbacks, and the climate benefits of forests. Science, 320(5882): 1444–1449.

Bormann K J, Brown R D, Derksen C, et al. 2018. Estimating snow-cover trends from space. Nature Climate Change, 8(11): 924–928.

Cess R D. 1978. Biosphere-albedo feedback and climate modeling. Journal of Atmospheric Sciences, 35(9): 1765–1768.

Chen C N, Tian L, Zhu L Q, et al. 2021. The impact of climate change on the surface albedo over the Qinghai-Tibet Plateau. Remote Sensing, 13(12): 2336, doi: 10.3390/rs13122336.

Deng X J, Jing C Q, Guo W Z, et al. 2021. Spatio-temporal variation characteristics of surface albedo and analysis of influential factors in the Junggar Basin. Arid Zone Research, 38(2):314–326. (in Chinese)

Dickinson R E. 1983. Land surface processes and climate—Surface albedos and energy balance. Advances in Geophysics, 25: 305–353.

Fan N, Xie G D, Zhang C S, et al. 2012. Spatial-temporal dynamic changes of vegetation cover in Lancang River Basin during 2001–2010. Resources Science, 34(7): 1222–1231. (in Chinese)

Fang H L, Liang S L, Kim H Y, et al. 2007. Developing a spatially continuous 1 km surface albedo data set over North America

from Terra MODIS products. Journal of Geophysical Research: Atmospheres, 112: D20206, doi: 10.1029/2006JD008377.

Fassnacht S R, Cherry M L, Venable N B H, et al. 2016. Snow and albedo climate change impacts across the United States Northern Great Plains. The Cryosphere, 10(1): 329–339.

Gascoin S, Ducharne A, Ribstein P, et al. 2009. Sensitivity of bare soil albedo to surface soil moisture on the moraine of the Zongo glacier (Bolivia). Geophysical Research Letters, 36(2): L02405, doi: 10.1029/2008GL036377.

Gomes L C, Faria R M, de Souza E, et al. 2019. Modelling and mapping soil organic carbon stocks in Brazil. Geoderma, 340: 337–350.

Gorelick N, Hancher M, Dixon M, et al. 2017. Google Earth Engine: Planetary-scale geospatial analysis for everyone. Remote Sensing of Environment, 202: 18–27.

Grömping U. 2009. Variable importance assessment in regression: linear regression versus random forest. The American Statistician, 63(4): 308–319.

He T, Liang S L, Yu Y Y, et al. 2013. Greenland surface albedo changes in July 1981–2012 from satellite observations. Environmental Research Letters, 8(4): 044043, doi: 10.1088/1748-9326/8/4/044043.

He T, Liang S L, Song D X. 2014. Analysis of global land surface albedo climatology and spatial-temporal variation during 1981–2010 from multiple satellite products. Journal of Geophysical Research: Atmospheres, 119(17): 10281–10298.

Hotaling S, Lutz S, Dial R J, et al. 2021. Biological albedo reduction on ice sheets, glaciers, and snowfields. Earth-Science Reviews, 220: 103728, doi: 10.1016/j.earscirev.2021.103728.

Hou W, Hou X Y. 2020. Spatial-temporal changes in vegetation coverage in the global coastal zone based on GIMMS NDVI3g data. International Journal of Remote Sensing, 41(3–4): 1118–1138.

Hou X Y, Wu T, Yu L J, et al. 2012. Characteristics of multi-temporal scale variation of vegetation coverage in the Circum Bohai Bay Region, 1999–2009. Acta Ecologica Sinica, 32(6): 297–304.

Huang W F, Cheng B, Zhang J R, et al. 2019. Modeling experiments on seasonal lake ice mass and energy balance in the Qinghai-Tibet Plateau: a case study. Hydrology and Earth System Sciences, 23(4): 2173–2186.

Kala J, Evans J P, Pitman A J, et al. 2014. Implementation of a soil albedo scheme in the CABLEv1.4b land surface model and evaluation against MODIS estimates over Australia. Geoscientific Model Development, 7(5): 2121–2140.

Knorr W, Schnitzler K G, Govaerts Y. 2001. The role of bright desert regions in shaping North African climate. Geophysical Research Letters, 28(18): 3489–3492.

Kong Y L, Pang Z H. 2012. Evaluating the sensitivity of glacier rivers to climate change based on hydrograph separation of discharge. Journal of Hydrology, 434–435: 121–129.

Li Q P, Ma M G, Wu X D, et al. 2018. Snow cover and vegetation-induced decrease in global albedo from 2002 to 2016. Journal of Geophysical Research: Atmospheres, 123(1): 124–138.

Li X J, Zhang H Y, Qu Y. 2020. Land surface albedo variations in Sanjiang Plain from 1982 to 2015: Assessing with glass data. Chinese Geographical Science, 30(5): 876–888.

Liang S L, Zhao X, Liu S H, et al. 2013. A long-term Global Land Surface Satellite (GLASS) data-set for environmental studies. International Journal of Digital Earth, 6(Supp1.): 5–33.

Liang S L, Wang D D, He T, et al. 2019. Remote sensing of earth's energy budget: Synthesis and review. International Journal of Digital Earth, 12(7): 737–780.

Liu Q, Wang L Z, Qu Y, et al. 2013. Preliminary evaluation of the long-term GLASS albedo product. International Journal of Digital Earth, 6(Supp1.): 69–95.

Liu S S, Yang Y H, Shen H H, et al. 2018. No significant changes in topsoil carbon in the grasslands of northern China between the 1980s and 2000s. Science of the Total Environment, 624: 1478–1487.

Liu Y H, Zhong Y F, Ma A L, et al. 2023. Cross-resolution national-scale land-cover mapping based on noisy label learning: A case study of China. International Journal of Applied Earth Observation and Geoinformation, 118: 103265, doi: 10.1016/j.jag.2023.103265.

Loranty M M, Berner L T, Goetz S J, et al. 2014. Vegetation controls on northern high latitude snow-albedo feedback: observations and CMIP5 model simulations. Global Change Biology, 20(2): 594–606.

Lucht W, Hyman A H, Strahler A H, et al. 2000. A comparison of satellite-derived spectral albedos to ground-based broadband albedo measurements modeled to satellite spatial scale for a semidesert landscape. Remote Sensing of Environment, 74(1): 85–98.

Luo N N, Bake B, Wu Y F. 2017. Analysis on spatiotemporal characteristics of drought-flood based on standard precipitation index in northern Xinjiang in recent 52 years. Research of Soil and Water Conservation, 24(2): 293–299. (in Chinese)

Malmros J K, Mernild S H, Wilson R, et al. 2018. Snow cover and snow albedo changes in the central Andes of Chile and Argentina from daily MODIS observations (2000–2016). Remote Sensing of Environment, 209: 240–252.

Moody E G, King M D, Schaaf C B, et al. 2007. Northern Hemisphere five-year average (2000–2004) spectral albedos of surfaces in the presence of snow: Statistics computed from Terra MODIS land products. Remote Sensing of Environment, 111(2–3): 337–345.

Ollinger S V, Richardson A D, Martin M E, et al. 2008. Canopy nitrogen, carbon assimilation, and albedo in temperate and boreal forests: Functional relations and potential climate feedbacks. Proceedings of the National Academy of Sciences, 105(49): 19336–19341.

Ouyang Z, Sciusco P, Jiao T, et al. 2022. Albedo changes caused by future urbanization contribute to global warming. Nature Communications, 13(1): 3800, doi: 10.1038/s41467-022-31558-z.

Pang G J, Chen D L, Wang X J, et al. 2022. Spatiotemporal variations of land surface albedo and associated influencing factors on the Tibetan Plateau. Science of the Total Environment, 804: 150100, doi: 10.1016/j.scitotenv.2021.150100.

Pearson R G, Phillips S J, Loranty M M, et al. 2013. Shifts in Arctic vegetation and associated feedbacks under climate change. Nature Climate Change, 3(7): 673–677.

Pistone K, Eisenman I, Ramanathan V. 2014. Observational determination of albedo decrease caused by vanishing Arctic sea ice. Proceedings of the National Academy of Sciences, 111(9): 3322–3326.

Planque C, Carrer D, Roujean J L. 2017. Analysis of MODIS albedo changes over steady woody covers in France during the period of 2001–2013. Remote Sensing of Environment, 191: 13–29.

Potts D R, Mackin S, Muller J P, et al. 2012. Sensor intercalibration over Dome C for the ESA GlobAlbedo project. IEEE Transactions on Geoscience and Remote Sensing, 51(3): 1139–1146.

Qu X, Hall A. 2007. What controls the strength of snow-albedo feedback? Journal of Climate, 20(15): 3971–3981.

Rangwala I, Miller J R. 2012. Climate change in mountains: a review of elevation-dependent warming and its possible causes. Climatic Change, 114(3): 527–547.

Rotenberg E, Yakir D. 2010. Contribution of semi-arid forests to the climate system. Science, 327(5964): 451–454.

Salomonson V V, Appel I. 2004. Estimating fractional snow cover from MODIS using the normalized difference snow index. Remote Sensing of Environment, 89(3): 351–360.

Sánchez-Granero M A, Trinidad-Segovia J E, García-Pérez J. 2008. Some comments on Hurst exponent and the long memory processes on capital markets. Physica A: Statistical Mechanics and its Applications, 387(22): 5543–5551.

Schaaf C B, Gao F, Strahler A H, et al. 2002. First operational BRDF, albedo nadir reflectance products from MODIS. Remote Sensing of Environment, 83(1–2): 135–148.

Shekhar M S, Chand H, Kumar S, et al. 2010. Climate-change studies in the western Himalaya. Annals of Glaciology, 51(54): 105–112.

Shi Q, Liang S. 2013. Characterizing the surface radiation budget over the Tibetan Plateau with ground-measured, reanalysis, and remote sensing data sets: 2. Spatiotemporal analysis. Journal of Geophysical Research: Atmospheres, 118(16): 8921–8934.

Song Y Z, Wang J F, Ge Y, et al. 2020. An optimal parameters-based geographical detector model enhances geographic characteristics of explanatory variables for spatial heterogeneity analysis: cases with different types of spatial data. GIScience & Remote Sensing, 57(5–6): 593–610.

Tang R Y, Zhao X, Zhou T, et al. 2018. Assessing the impacts of urbanization on albedo in Jing-Jin-Ji Region of China. Remote Sensing, 10(7): 1096, doi: 10.3390/rs10071096.

Tang X Y, Cui Y P, Li N, et al. 2020. Human activities enhance radiation forcing through surface albedo associated with vegetation in Beijing. Remote Sensing, 12(5): 837, doi: 10.3390/rs12050837.

Van De Kerchove R, Lhermitte S, Veraverbeke S, et al. 2013. Spatio-temporal variability in remotely sensed land surface temperature, and its relationship with physiographic variables in the Russian Altay Mountains. International Journal of Applied Earth Observation and Geoinformation, 20: 4–19.

Verheijen F G A, Jeffery S, van der Velde M, et al. 2013. Reductions in soil surface albedo as a function of biochar application rate: implications for global radiative forcing. Environmental Research Letters, 8(4): 044008, doi: 10.1088/1748-9326/8/4/044008.

Wang J F, Xu C D. 2017. Geodetector: Principle and prospective. Acta Geographica Sinica, 72(1): 116–134. (in Chinese)

Wang J J, Ding J L, Zhang Z. 2019. Temporal-spatial dynamic change characteristics of soil moisture in Ebinur Lake Basin from 2008–2014. Acta Ecologica Sinica, 39(5): 1784–1794. (in Chinese)

Wang K C, Wang P C, Liu J M, et al. 2005. Variation of surface albedo and soil thermal parameters with soil moisture content at

a semi-desert site on the western Tibetan Plateau. Boundary-Layer Meteorology, 116(1): 117–129.

Wang X W, Xie H J, Liang T G. 2008. Evaluation of MODIS snow cover and cloud mask and its application in Northern Xinjiang, China. Remote Sensing of Environment, 112(4): 1497–1513.

Wang Y F, Shen Y J, Sun F B, et al. 2014a. Evaluating the vegetation growing season changes in the arid region of northwestern China. Theoretical and Applied Climatology, 118: 569–579.

Wang Z S, Schaaf C B, Chopping M J, et al. 2012. Evaluation of Moderate-resolution Imaging Spectroradiometer (MODIS) snow albedo product (MCD43A) over tundra. Remote Sensing of Environment, 117: 264–280.

Wang Z S, Schaaf C B, Strahler A H, et al. 2014b. Evaluation of MODIS albedo product (MCD43A) over grassland, agriculture and forest surface types during dormant and snow-covered periods. Remote Sensing of Environment, 140: 60–77.

Wen J G, Lin X W, Wu X D, et al. 2022. Validation of the MCD43A3 collection 6 and GLASS V04 snow-free albedo products over rugged terrain. IEEE Transactions on Geoscience and Remote Sensing, 60: 5632311, doi: 10.1109/TGRS.2022.3214103.

Wielicki B A, Wong T, Loeb N, et al. 2005. Changes in Earth's albedo measured by satellite. Science, 308(5723): 825, doi: 10.1126/science.11064.

Xu H Q. 2009. Quantitative analysis on the relationship of urban impervious surface with other components of the urban ecosystem. Acta Ecologica Sinica, 29(5): 2456–2462.

Xu Z Y, Qiu X F, Li S S, et al. 2020. Analysis of surface albedo over China based on MODIS. Journal of Arid Land Resources and Environment, 34(1): 99–105. (in Chinese)

Zhang H W, Song J, Wang G, et al. 2021a. Spatiotemporal characteristic and forecast of drought in northern Xinjiang, China. Ecological Indicators, 127: 107712, doi: 10.1016/j.ecolind.2021.107712.

Zhang Y, Chu X Z, Yang S M, et al. 2019. Climate change in North Xinjiang in recent 56 years. Arid Zone Research, 36(1): 212–219. (in Chinese)

Zhang Y L, Gao T G, Kang S C, et al. 2021b. Albedo reduction as an important driver for glacier melting in Tibetan Plateau and its surrounding areas. Earth-Science Reviews, 220: 103735, doi: 10.1016/j.earscirev.2021.103735.

Zhao Z C, Zhao K, Xu J B, et al. 2014. Spatial-temporal changes of surface albedo and its relationship with climate factors in the source of three rivers region. Arid Zone Research, 31(6): 1031–1038. (in Chinese)

Zou L, Gao F, Ma Y J. 2021. Spatial distribution of water quality in Ulungur Lake. Journal of Hydroecology, 42(1): 35–41. (in Chinese)